RAMTRANS Vol. 14, No. 1, pp. 49–61 (2003)
Published by Nuclear Technology Publishing

THE USE OF CASTOR OIL POLYURETHANE FOAM IN IMPACT LIMITERS FOR RADIOACTIVE MATERIALS PACKAGES

R. P. Mourão† and M. M. Neto‡
†Centro de Desenvolvimento da Tecnologia Nuclear
Comissão Nacional de Energia Nuclear
Belo Horizonte, MG, Brazil
‡Instituto de Pesquisas Energéticas e Nucleares
Comissão Nacional de Energia Nuclear
São Paulo, SP, Brazil

Received January 2 2003, amended April 25 2003, accepted May 2 2003

Abstract — This paper presents ongoing research aiming to assess the use of a 'bio based' polyurethane foam as filling material in impact limiters for transport packages in the nuclear field. The foam is made from castor oil, which replaces the petroleum based polyols in the manufacture of polyurethane products, with good environmental advantages. The research comprises the selection of the cellular material, its structural characterisation by mechanical laboratory tests, the development of a case study, preliminary determination of the best foam density for the case study, performance of the case and its numerical simulation using the finite element method. Prototypes with foam density that is pre-determined as ideal, as well as prototypes using lighter and heavier foams, were tested for comparison. The results obtained validate the research methodology, as expectations about the ideal foam density were confirmed by the drop tests and the numerical simulation.

INTRODUCTION

Impact limiters have been extensively used among designers of packages in the nuclear field[1–5]. These sacrificial components are added to the packages to absorb and dissipate energy in impact events and to act as thermal barriers in accidents involving fire. Several impact limiter configurations have been proposed and different filling materials studied, such as natural or reconstituted wood, light concrete, metallic and polymeric foams and aluminium honeycomb. These materials are collectively known as cellular materials.

A much studied configuration is made of a thin metallic shell with polyurethane foam filling. The advantages offered by this arrangement are simple fabrication, good specific energy absorption characteristics, low anisotropy, low costs and effective thermal protection.

In Brazil, a polyurethane foam produced from the castor plant, *Ricinus communis*, is replacing the pet-

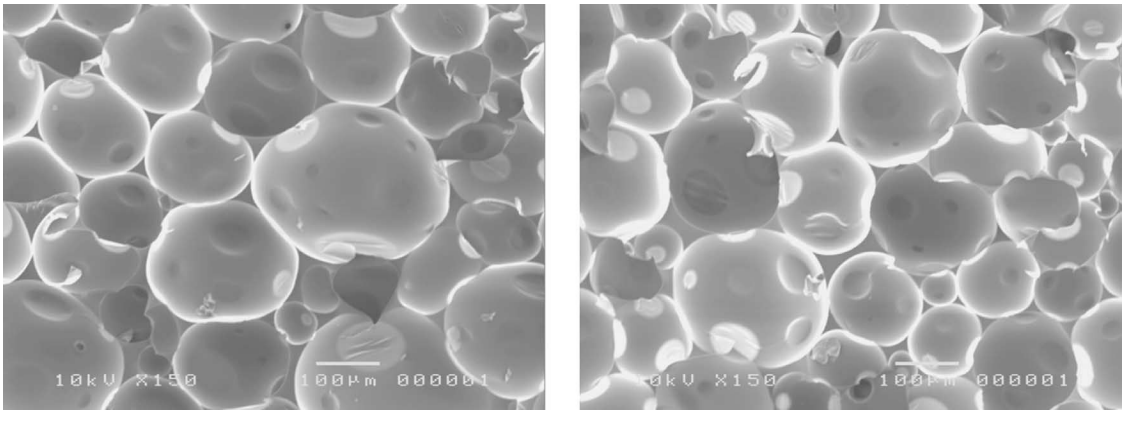

Figure 1. Scanning electron microscopy images of a castor oil foam with density of $\rho = 165$ kg m^{-3} (magnification: ×150).

Contact author E-mail: mouraor@cdtn.br

roleum based one, with evident environmental benefits, as it is produced from a plant based, renewable resource and does not require the use of a gaseous chlorofluorocarbon (CFC) during its manufacture. Also, this product is available locally and its cost is no higher than the traditional one that it is intended to substitute. It lacks, however, a systematic characterisation programme, which would enable it to be used as a structural element for package protection.

This paper presents the results obtained so far in research carried out to verify the feasibility of using this material in the protection of radioactive material transport packages. The methodology used comprises the selection of the cellular material and its characterisation through mechanical laboratory tests; the use of a method for characterising the foam energy absorption capacity; the development of a case study, namely the performance of the regulatory 9 m drop test; and its numerical simulation using the finite element method.

CELLULAR MATERIAL SELECTION AND CHARACTERISATION

As previously stated, among the cellular materials most commonly used as impact limiter filling, the castor oil polyurethane foam was chosen to be studied in this research. Its good mechanical properties, environmently friendly characteristics and local availability led to this selection. As no strict material ranking was actually carried out during this phase of the research, a comparative study will be made later involving other potentially promising materials, especially reconstituted wood and light cement.

Experimental characterisation of castor oil foam

The characterisation of the castor oil foam was carried out through the study of its microstructure and the performance of laboratory physical tests. An image

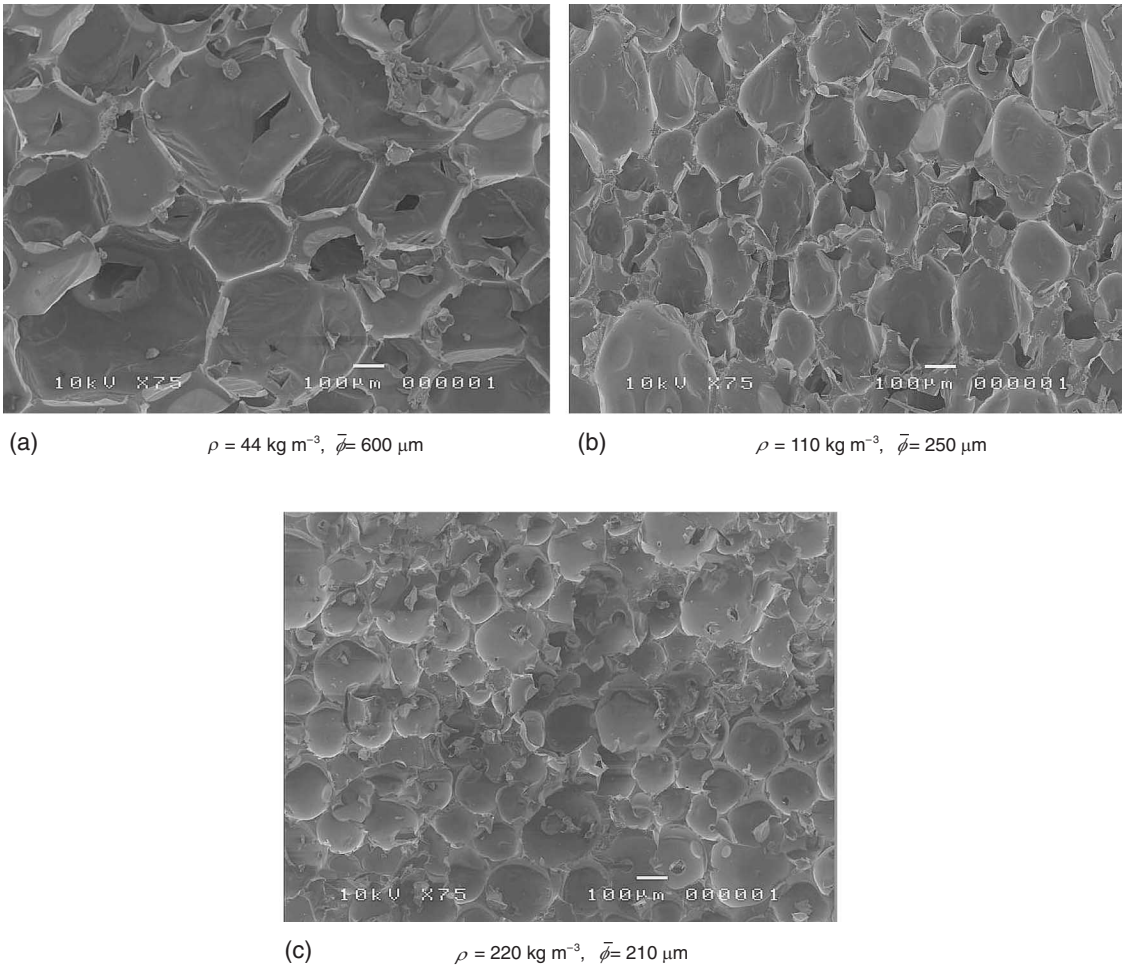

Figure 2. Cell size dependence on density (magnification: ×75).

based analysis using a scanning electron microscope was conducted to obtain direct visual images of the cell geometry of undeformed foam specimens and to verify whether this foam cell shape could be modelled by one of the geometrical models proposed in the literature[6–8]. As regards the laboratory tests, the complete mechanical characterisation of the foam, for the purpose of this research, was obtained by carrying out uniaxial and hydrostatic quasi-static tests and impact tests.

Microstructure of the castor oil foam

Figure 1 shows the scanning electron microscopy images of a 165 kg m^{-3} castor oil foam, taken both in the parallel and perpendicular directions*. It can be seen that the cells are completely closed (some polymeric materials yield open celled foams), have a fairly spherical shape and connect to several neighbouring cells. The cell surface is smooth and suffers pressure from the contacting cells during foam formation, as can be seen from the dents observed on the surfaces of the front cells.

Figure 2 shows the correlation observed between cell size and density. It can be seen that the greater the density, the smaller the average cell diameter, $\overline{\phi}$; this relationship was indeed expected, given that bigger cells have greater volume-to-mass ratios, thus producing lighter foams.

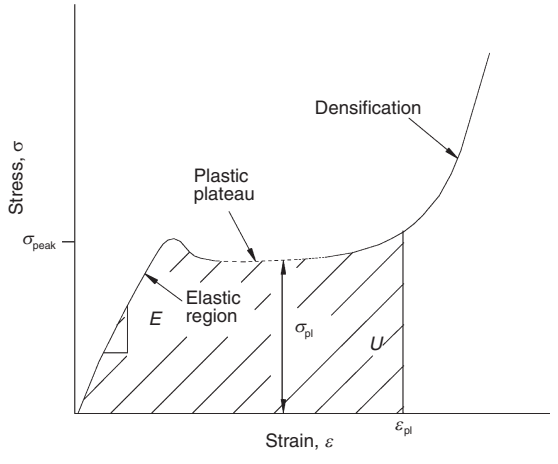

Figure 3. Stress–strain curve for foam deformation in uniaxial compression test.

LABORATORY TESTS

The parameters determined in the foam testing programme were Young's modulus E, Poisson's ratio ν, the specific energy absorption U, the peak and plateau stresses σ_{peak} and σ_{pl} and the plateau deformation ϵ_{pl}, as shown in Figure 3, which depicts a typical stress–strain curve obtained in a uniaxial compression test. Initially, the foam shows elastic behaviour at low stresses, which is followed by a long plateau where the plastic collapse of the foam cell takes place, until the onset of the foam densification, which is characterised by the compaction of the foam solid skeleton and expelling of the air initially existing in and between the cells. The average

* The polymeric foam expands considerably during the chemical reaction that occurs during its formation, undergoing a several-fold increase in its original volume. If this expansion is restricted in two directions (as occurs, for instance, inside a rigid mould), these directions are referred to as *perpendicular* directions and the free foam 'rising' direction is denoted as the *parallel* direction.

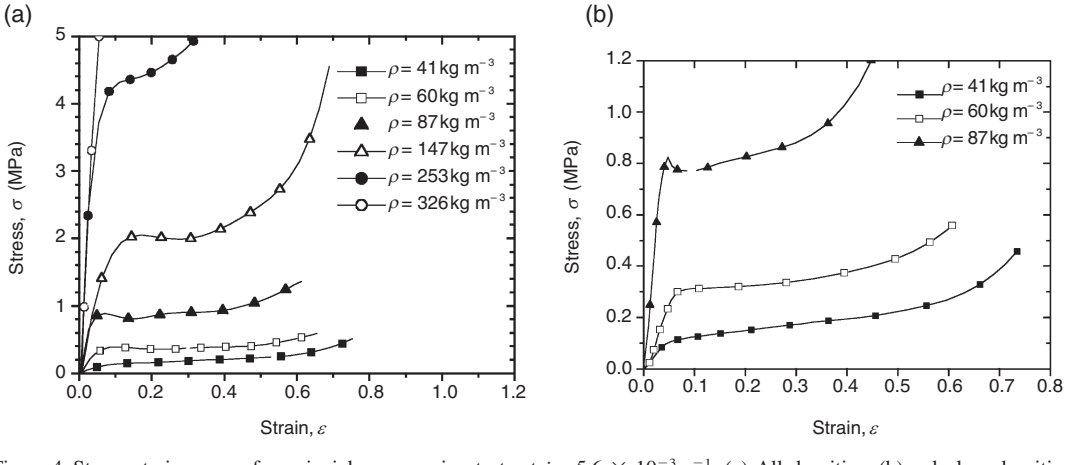

Figure 4. Stress–strain curves for uniaxial compression tests at $\dot{\epsilon} = 5.6 \times 10^{-3}$ s^{-1}. (a) All densities; (b) only low densities.

slope of the curve in the elastic region corresponds to E and the average stress of the plateau is σ_{pl}. The value of deformation at the transition between the plateau and the densification regime is ϵ_{pl}. The energy absorbed by the foam per unit volume, U, at a certain strain ϵ is the area under the curve up to this deformation.

Sometimes, a sudden drop in foam strength is observed at the transition between the elastic and the plastic regimes. The maximum stress value recorded at this moment is σ_{peak}. In the present study, this phenomenon was detected when specimens of foams with densities of around 80 kg m^{-3} were tested in the parallel direction.

The uniaxial compression test was carried out according to the standard ASTM-D-1621, *Compressive strength of rigid cellular plastics*[9]. The following foam densities were tested: 41, 60, 87, 147, 253 and 326 kg m^{-3}. The test consisted of subjecting specimens to compression in a universal tension/compression machine. The specimens had 50 mm $\times$ 50 mm square cross section and 60 mm in height. The test (crosshead) velocities were set at 5, 20 and 50 mm min^{-1}, yielding strain rates of $\dot{\epsilon} = 1.4 \times 10^{-3}$, 5.6×10^{-3} and 1.4×10^{-2} s^{-1}, respectively. In order to study the foam isotropy, specimens taken in both the parallel and perpendicular directions to the foam's rising direction were tested.

The results obtained are shown in Figures 4–7. It was observed that the behaviour of castor oil foam in deformation is similar to that of the petroleum based foam (similar curve shape and similar dependency rules of foam parameters on density). This finding is very important in that it legitimises, for the studied foam, the use of the constitutive models and methods of characterising the foam energy absorption capacity originally developed for the petroleum based foams.

Figure 5 shows the variation in the foam's main parameters (E, σ_{pl} and U); dependence of the foam density is shown, as well as a comparison with the parameters of a modified petroleum based foam developed by

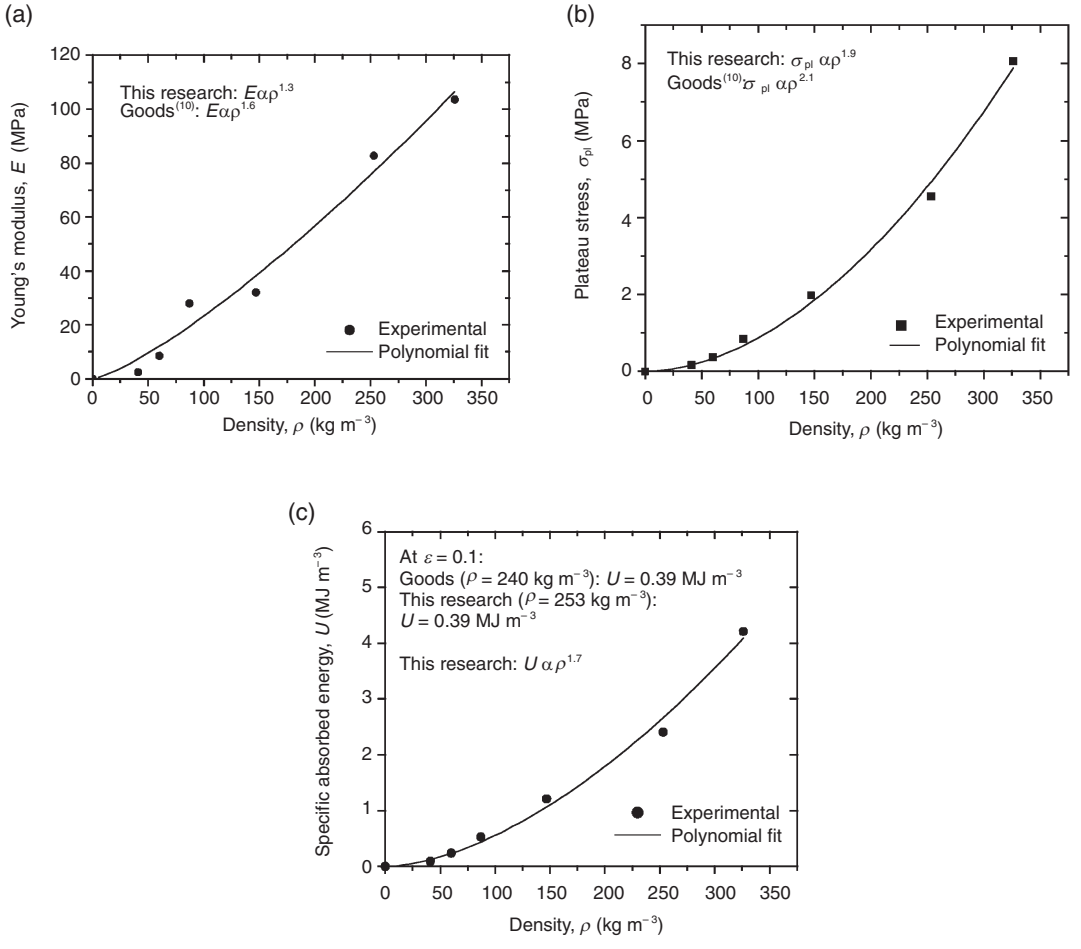

Figure 5. The dependence of foam parameters on density (results from uniaxial compression tests).

Table 1. Dynamic test parameters.

Foam density (kg m^{-3})	Drop weight (kg)	Drop height (m)	Strain rate (s^{-1})
43	19.4	0.56	130
60	19.4	0.57	132
		0.65	141
		0.73	149
108	48.45	1.20	191
165	43.45	1.94	243
229	43.45	2.11	253
		2.27	263
		3.32	318
277	48.45	3.32	318

Goods *et al*[10]. All parameters of the castor oil foam presented an exponential variation with density, as shown in Figure 5 (a)–(c). The exponential laws for E and σ_{pl} were compared, with good agreement, with those obtained by Goods *et al*. The value of U at 0.1 (10%) strain for the 253 kg m^{-3} castor oil foam was compared with the same parameter at the same strain for the 240 kg m^{-3} foam studied by Goods *et al*. The values were found to be exactly the same: $U = 0.39$ MJ m^{-3}.

The strain rate dependence of the castor oil foam strength is depicted in Figure 6. The low density foam (ρ = 41 kg m^{-3}) has a remarkable sensitivity to $\dot{\epsilon}$, increasing its stiffness with the strain rate. On the other hand, the high density foam (ρ = 253 kg m^{-3}) shows little sensitivity to this parameter.

Figure 7 shows the way in which the foam anisotropy varies with the foam density. Foams with densities of up to 180–200 kg m^{-3} have greater U and σ_{pl} values when tested in the parallel direction, whereas for foams with higher densities, these parameters have greater values when the specimens are compressed in the perpendicular direction. It is worth noting that the anisotropy presented can be considered mild; foams in the 180–200 kg m^{-3} density range are indeed practically isotropic.

The hydrostatic test was carried out using apparatus consisting of a water filled, piston provided, pressure chamber and a universal tension/compression machine. The specimens were initially jacketed in thin latex pouches and inserted into the chamber, which was positioned on the universal machine base. The hydrostatic pressure was established by the chamber piston being pressed down by the machine's head. As water is incompressible, for practical purposes, all reductions in the volume of the internal space of the chamber (measured by the displacement of the machine's head) corresponds to the volumetric strain of the specimen. The following foam densities were tested: 44, 56, 108, 143 and 259 kg m^{-3}. These densities do not match the ones used for the previous uniaxial test because they were produced from different foam blocks. In both cases, however, the density range allowed for a sound statistical treatment of the results obtained. The volumetric strain rates were set to $\dot{\epsilon}_v = 1.8 \times 10^{-3}$, 4.5×10^{-3} and 9.0×10^{-3} s^{-1}.

The response of the castor oil foam under hydrostatic pressure follows the same pattern as that observed during the uniaxial compression. As can be seen in Figure 8, in this test, also, the foam undergoes three very distinct phases during deformation: initial elastic, plastic plateau and densification. Also similarly to the previous test, σ_{pl} and U vary exponentially with density.

Finally, the response of the studied foam to dynamic

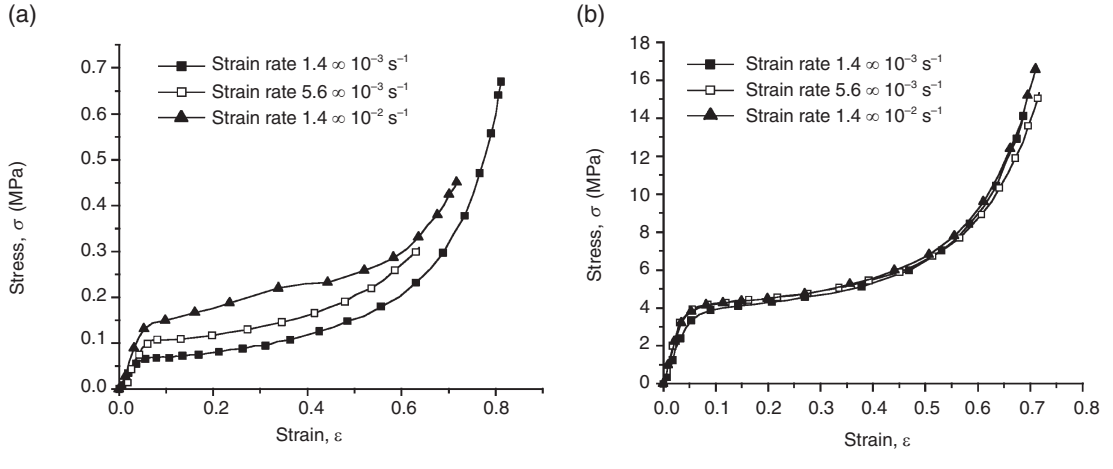

Figure 6. Strain rate dependence of the stress–strain curve for foams of two densities (uniaxial compression tests). (a) $\rho = 41$ kg m^{-3}; (b) $\rho = 253$ kg m^{-3}.

loads was assessed through impact tests, carried out according to the ASTM-D-1597 standard, *Shock-absorbing characteristics of package-cushioning materials*[11]. The test specimens consisted of square prisms with a 100 mm × 100 mm cross section by 25.4 mm thickness, taken from the parallel and perpendicular foam rising directions. The foam densities tested were 43, 60, 108, 165, 229 and 277 kg m^{-3}.

The test apparatus consisted of a 3.5 m high tubular frame provided with a rigid dropping weight, a strain gauge type load cell and an unyielding anvil. The test consisted of releasing the weight from different heights onto fresh specimens resting on the anvil. The mass of the dropping weight could be varied in such a way that suitable mass–drop height combinations could be obtained for each tested density. The load readings obtained as voltage signals were acquired and stored using an adequate electronic system with conditioning unit and oscilloscope working with electronic simulation computer software. These signals were internally converted into units of force and, given that the dropping mass was known, the accelerations during the impact could be determined. Table 1 shows the main parameters of the dynamic tests carried out; it can be noted that the strain rate varies from 130 to 318 s^{-1}.

The dynamic response of the studied foam is shown in Figure 9. The stress–strain curves obtained in the impact tests have the same shape as those from the quasi-static compression tests. However, a visible oscillation is presented by the curves in this case, which is expected in short duration dynamic events.

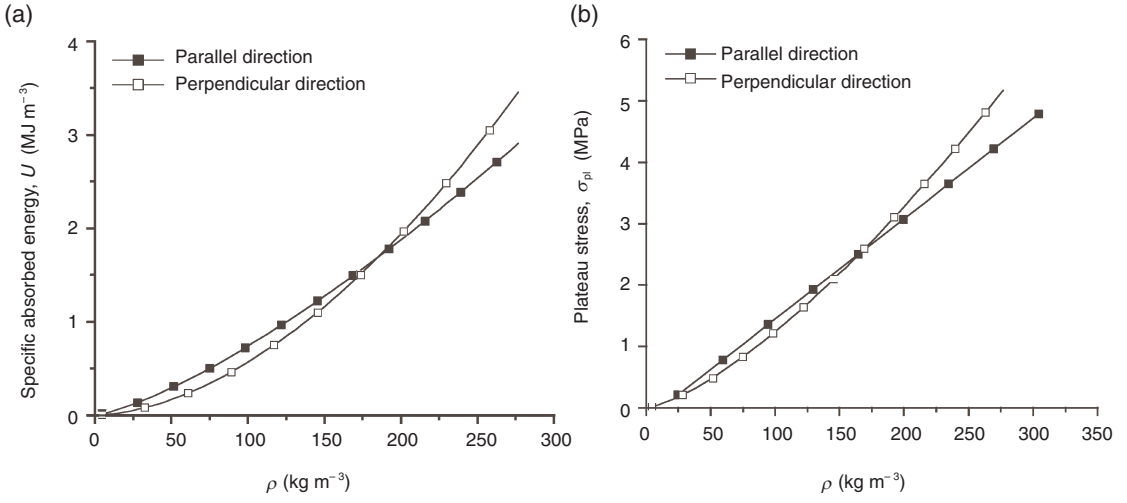

Figure 7. Dependence of foam anisotropy on density.

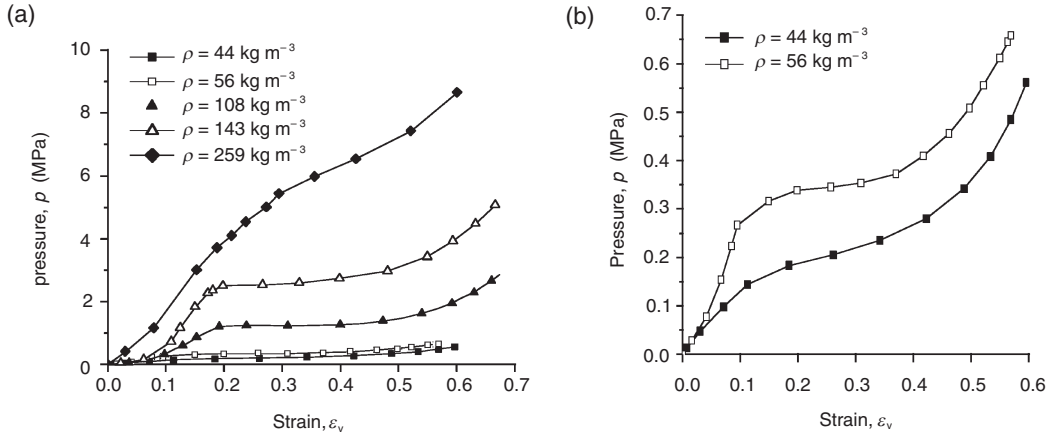

Figure 8. Pressure–strain curves. (a) All foam densities; (b) only lower foam densities.

CASE STUDY: 9 m FREE DROP TEST

The performance of the castor oil foam for protection against impact was verified by submitting package prototypes to the regulatory 9 m free drop test[12]. The simulated package was made up of two components: the main body and the impact limiter (Figure 10). The former consists of a 200 litre metallic drum filled with a massive concrete block with a mass of 500 kg (approximately 80 kg of steel balls were added to the lower half of the block to increase the prototype stability). The latter consists of a foam filled 1 mm thick carbon steel shell provided with a foam injection opening and eyelets for attachment to the main body.

Four geometrically similar impact limiters were tested, filled with foams with the following densities*: 41, 101, 117 and 225 kg m^{-3}. As will be shown in the following session, two prototypes were filled with

* The commercially available foam densities are 40, 100 and 200 kg m^{-3}. These are, however, nominal densities and some variation due to environmental temperature, humidity and also mould temperature is expected.

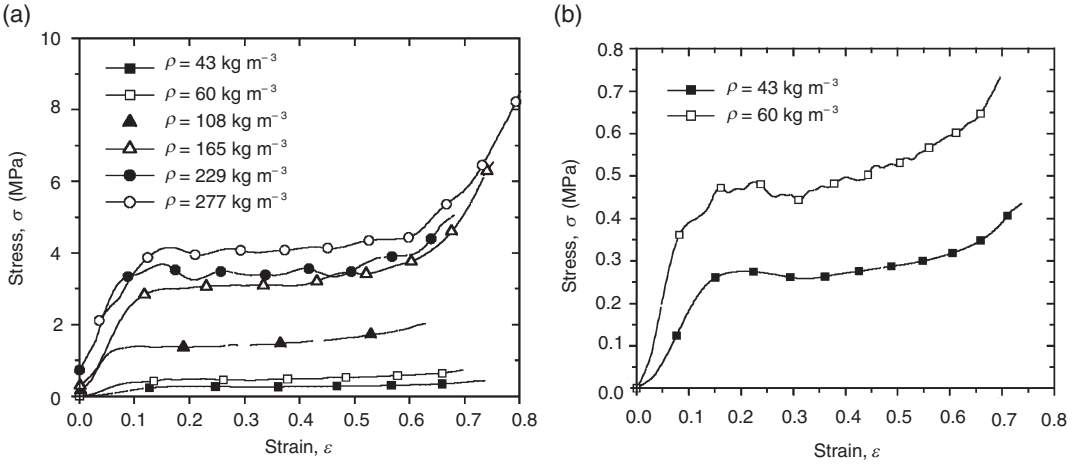

Figure 9. Results of the impact test. (a) All foam densities; (b) only lower foam densities.

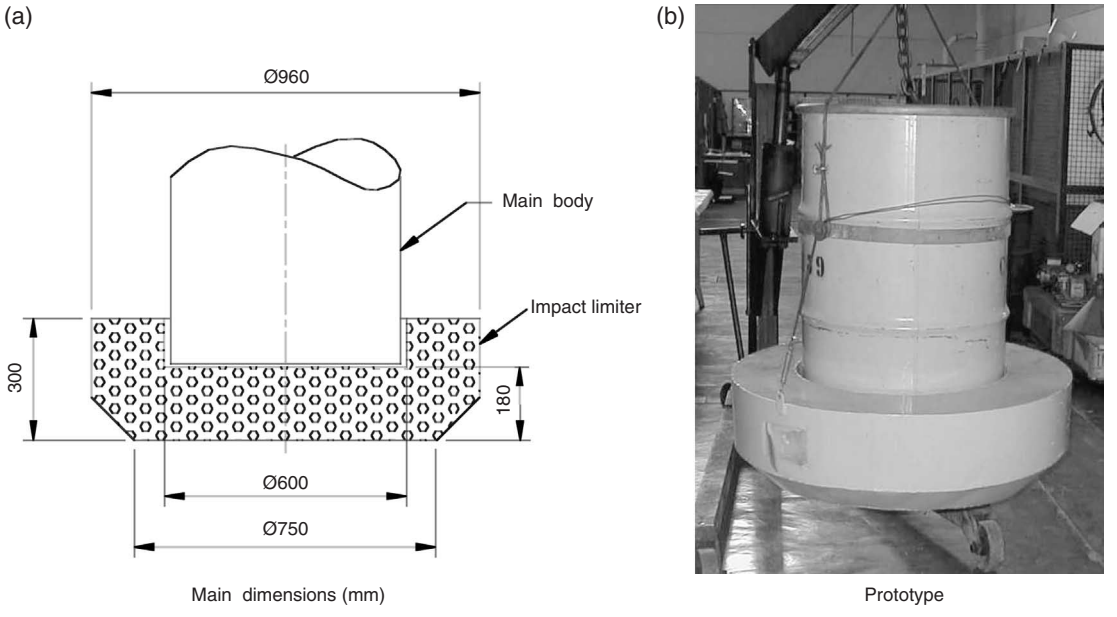

Figure 10. Package prototype.

foams with densities near those considered optimal by a method for characterising the foam energy absorption capacity (101 and 117 kg m^{-3}), one with a density below this value (41 kg m^{-3}) and one with a density above the optimal one (225 kg m^{-3}). All prototypes were tested in the vertical position.

The Janssen factor method

For the majority of impact problems, the most desired scenario is one in which the cushioning material absorbs and dissipates the largest amount of energy while transmitting the least possible effects to the protected item. Referring to Figure 3, this situation is observed when the foam deforms up to the end of the plastic plateau (corresponding to the foam deformation ϵ_{pl}); beyond this point, the disadvantages due to the sharp increase in stress in the foam (and, consequently, in the package) will outweigh the benefits of the additional energy absorbed.

The Janssen factor method, originally developed by Woolam[13] as a means of measuring the efficiency of a cushioning material in absorbing a certain amount of energy (by comparing it with the efficiency of an ideal absorber), is a straightforward method for estimating the performance of a cellular material in a given application. In dynamic testing, this factor can be defined as the ratio of the stress in the material to the specific energy absorbed:

$$J = \frac{\sigma}{U} \tag{1}$$

For a certain σ–ϵ curve obtained during an impact test, it is possible to construct a corresponding *J*–*U* curve. In his study, Woolam observed that this curve was U-shaped and that the minimum corresponds to the maximum efficiency of the tested material. In applying this method to forecast the most efficient foam density for the case study considered, the first step was to determine the value of the energy to be absorbed by the impact limiter. Disregarding the contribution of the metallic shell, considering that the active foam volume was the one below the vertical projection of the prototype's main body, and considering the following parameters:

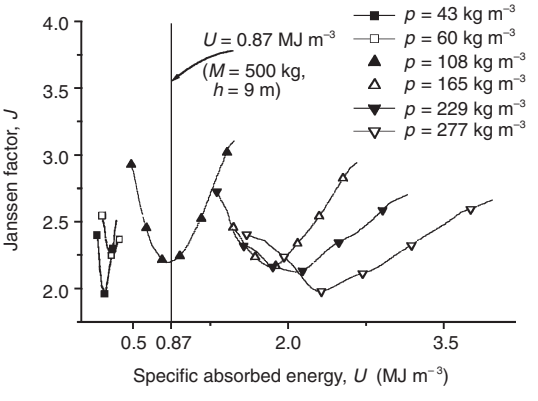

Figure 11. *J*–*U* curves for the foam densities tested (laboratory impact test).

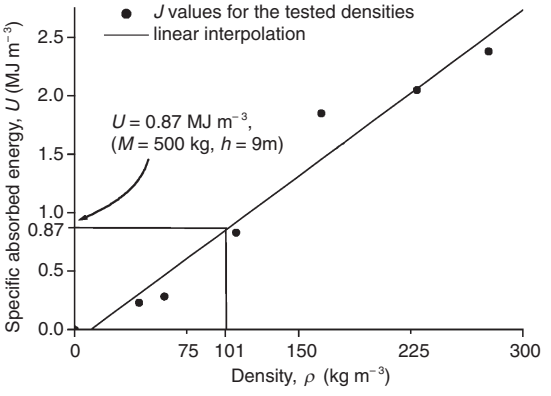

Figure 12. Interpolation of the minimum *J* values (laboratory impact test).

Figure 13. Prototype positioned for the drop test.

(1) foam active volume, $V = 5.1 \times 10^{-2}$ m^3 (projected area: 0.28 m^3; thickness: 0.18 m), and
(2) prototype kinetic energy, $E = \frac{1}{2} mv^2 = \frac{1}{2} \times 500$ kg $\times (13.3 \text{ m s}^{-1})^2 = 4.42 \times 10^{-2}$ MJ,

the energy absorbed per foam volume is:

$$U = \frac{E}{V} = \frac{4.42 \times 10^{-2} \text{ MJ}}{5.1 \times 10^{-2} \text{ m}^3} = 0.87 \text{ MJ m}^{-3}. \quad (2)$$

The next step was the construction of the *J–U* curves, based on the existing impact test σ–ϵ curves. The last step was the selection of the most appropriate foam density. Figure 11 depicts the *J–U* curves obtained and Figure 12 the linear interpolation of the minimum *J* values. As can be observed, the most efficient foam density for the case study carried out is 101 kg m^{-3}.

Results of the free drop test

The drop tests were carried out at the package testing facility at the Centro de Desenvolvimento da Tecnologia Nuclear (CDTN) (Figure 13). The registered parameter was the acceleration during impact, recorded at the central point of the upper surface of the concrete block.

The results of the drop tests are shown in Figure 14 and Table 2. The smallest acceleration peak (68 g) was recorded for the 101 kg m^{-3} foam, followed by the foam with 117 kg m^{-3} density, which registered 86 g. These results are in full agreement with the forecast made by the Janssen factor method.

Table 2. Maximum acceleration peaks during the drop tests.

Foam density (kg m^{-3})	Maximum peak (g)
41	159
101	68
117	86
225	122

NUMERICAL SIMULATION OF THE DROP TEST

The free drop tests carried out in this research were numerically simulated by the finite element method. The computer code ANSYS LS-DYNA[14,15] was used, due to its robustness in solving impact problems involving large deformations and displacements and complex contact conditions, and because there are several foam models implemented in its material model library.

DESCRIPTION OF THE MODEL

Figure 15 shows the finite element model used. As can be seen in Figure 15(a), only one quarter of the prototype was modelled, due to the existing geometric and loading symmetries (the prototypes were tested in the vertical position). In order to save processing time, the prototype was positioned in contact with the platform and an initial vertical velocity of 13.3 m s^{-1} was imposed on it.

Table 3. Main parameters of the model.

Part	Material formulation	Element type	Number of elements/nodes
Main body	Rigid body	SOLID164	81/148
Polymeric foam	Crushable foam	SOLID164	1.215/327
Metallic cask	Plastic kinematic	SHELL163	198/235
Unyielding base	Rigid body	SHELL163	1/4
		TOTAL	1.495/714

Table 4. Comparison between maximum accelerations.

Foam density (respectively, experimental and in the numerical simulation) (kg m^{-3})	a_{max}, numerical simulation (g)	a_{max}, experimental (g)	Difference (%)
41, 60	151	159	−5
101, 104	107	68	57
117, 104		86	24
225, 200	135	122	11

Figure 15(b)–(e) depict the individual parts of the model. The model's main parameters are shown in Table 3. A method deviation worth noting is the simulation of the 41 kg m^{-3} foam by a 60 kg m^{-3} foam. This non-conformity was introduced because the tentative use of the foam model most adequate for low density foams — the closed cell foam model — led to numerical instabilities due to the excessive impact limiter's deformation (more than 85%). The crushable foam model used instead is adequate for the 60 kg m^{-3} but not for the 41 kg m^{-3} foam. It is also worth noting that the tested 101 and 117 kg m^{-3} foams were compared with the numerically simulated 104 kg m^{-3} foam and the tested 225 kg m^{-3} foam with the simulated 200 kg m^{-3}. As the σ–ϵ curve in the uniaxial test is input data for the foam model in the numerical simulation, the densities used were selected among those tested in this test (see Figure 4(a)), bearing in mind that averaged values of these densities were also used (for instance, the input σ–ϵ curve for the 104 kg m^{-3} foam was obtained as an average of the curves of 60 and 147 kg m^{-3} foams). For the purpose of this research, the above described deviation did not invalidate the use of the numerical simulation, since the cases still simulated foams with density pre-determined as ideal, as well as lighter and heavier foams.

RESULTS

The results of the numerical simulation are shown in Figures 16–20. In Figure 16, the pulses of acceleration during the impact for all foam densities are plotted against time. It can be seen that the prototype using the foam density near the one deemed ideal (104 kg m^{-3}) yielded the lowest acceleration peak (107 g), followed by the one using the 200 kg m^{-3} foam (135 g), while the lightest foam (60 kg m^{-3}) yielded the highest acceleration (with a maximum value of 151 g). These results match the prediction of the Janssen factor method.

Figures 17–20 and Table 4 compare experimental and numerical peak accelerations for the individual prototypes tested. The differences observed in the peak accel-

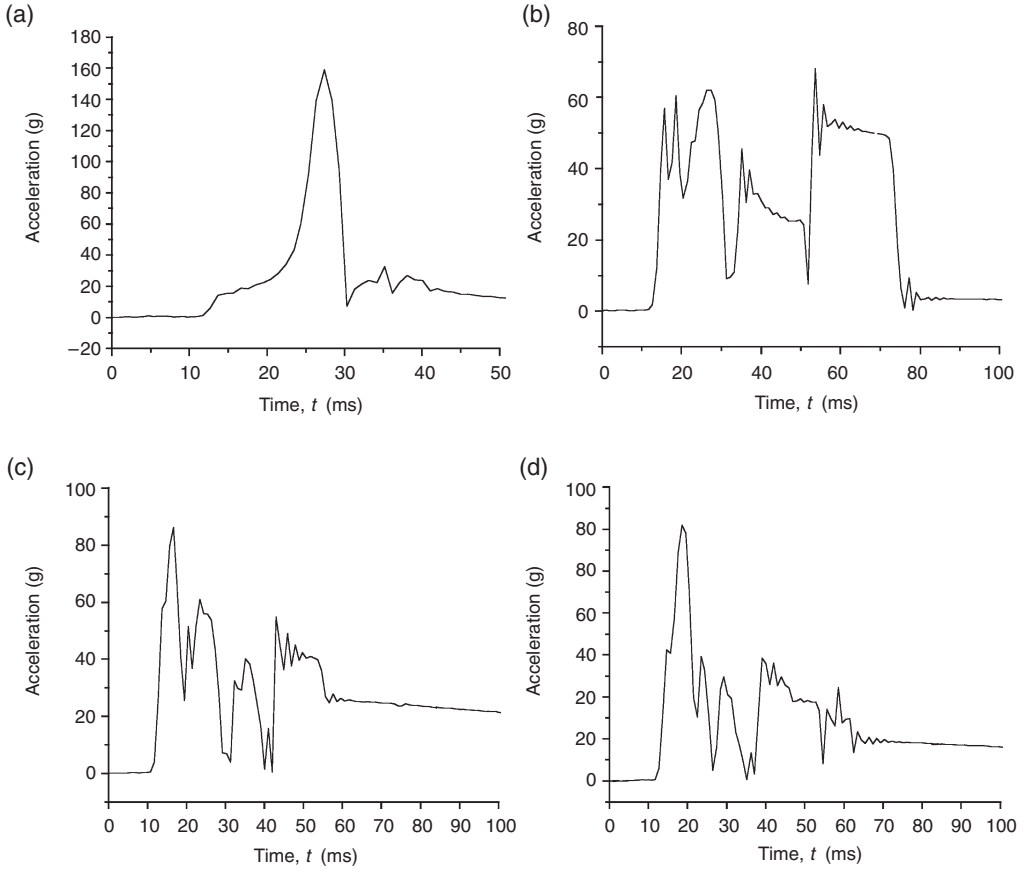

Figure 14. Acceleration curves for the tested prototypes. The densities, ρ, are: (a) 41 kg m^{-3}; (b) 101 kg m^{-3}; (c) 117 kg m^{-3}; and (d) 225 kg m^{-3}.

erations (up to 57%) may be caused by the fact that the stress–strain curves used as input for the foam model are curves from the uniaxial compression tests, carried out under strain rates in the range 10^{-3}–10^{-2} s^{-1}, whereas, in the simulated drop test, the foam is compressed at an initial strain rate of around 74 s^{-1}. However, no confirmatory study has been carried out on this subject.

CONCLUSIONS

The castor oil based polyurethane foam has basically the same mechanical properties as the traditional petroleum based foams. Because of that, the constitutive models and mathematical methods for characterising the foam energy absorption capacity developed for the latter are also valid for the studied foam. Other favourable

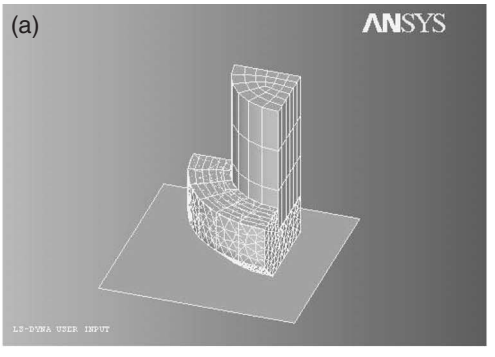

Complete model

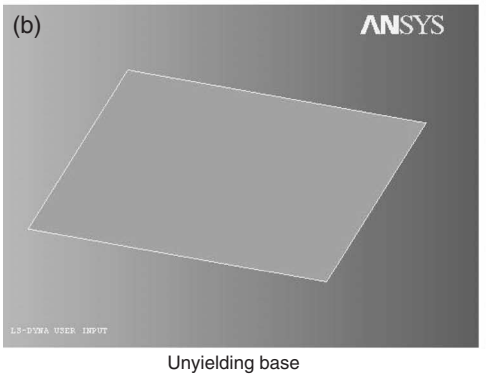

Unyielding base

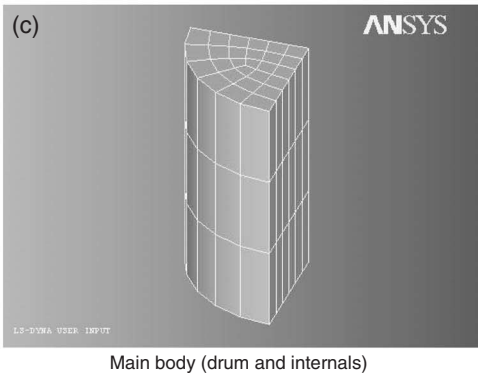

Main body (drum and internals)

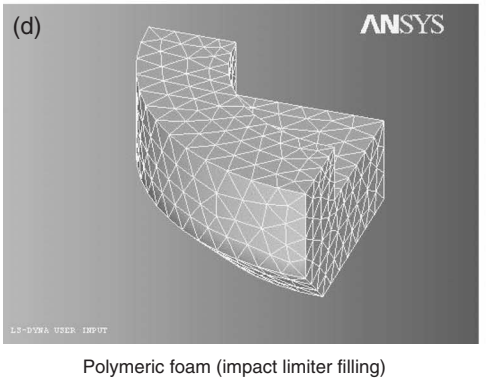

Polymeric foam (impact limiter filling)

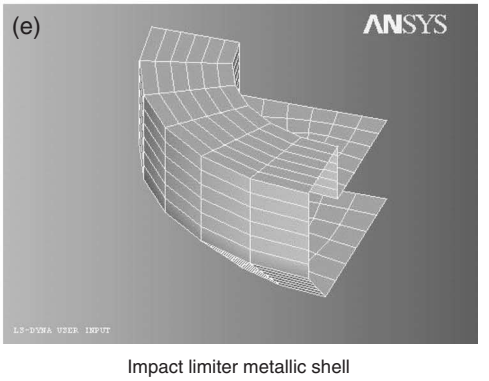

Impact limiter metallic shell

Figure 15. Finite element model.

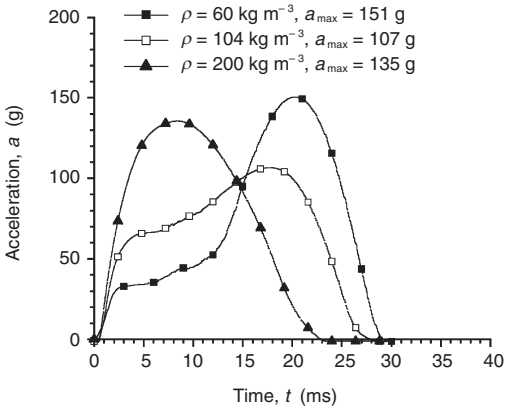

Figure 16. Acceleration pulse during impact — numerical simulation.

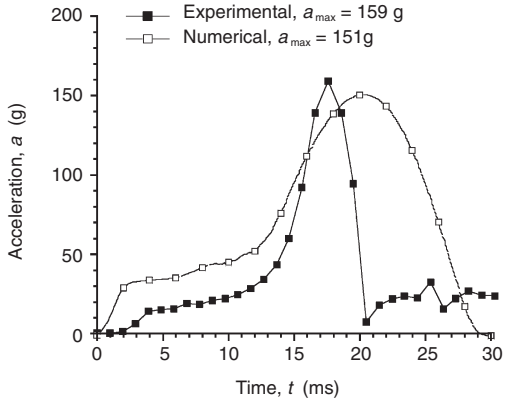

Figure 17. Comparison between experimental and numerical data for the foam of density below the value calculated as optimal by the Janssen factor method: 41 kg m^{-3} (experimental) and 60 kg m^{-3} (numerical.)

characteristics of this material which make it attractive as filling material in impact limiters are its mild anisotropy (and even a near isotropy at the density range 180–200 kg m^{-3}), easy manufacture, availability in the local Brazilian market (and therefore, low costs) and, above all, its good energy absorption and dissipation capacity. From the environmental point of view, this foam presents the indisputable advantage of being produced from a renewable resource and not requiring the use of a CFC in its manufacture.

The methodology used in this research, comprising (1) the selection of the cellular material; (2) its structural characterisation by laboratory tests; (3) the development of a case study — a regulatory 9 m drop test; (4) the preliminary determination of the best foam density for the case study using a method of characterising energy absorption in foams; and (5) the numerical simulation of the case by the finite element method, was found to

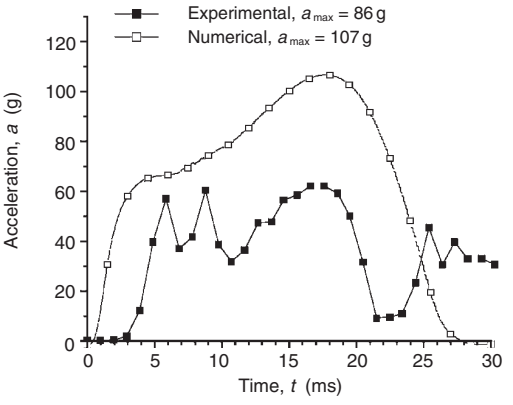

Figure 18. Comparison between experimental and numerical data for the foam of optimal density: 101 kg m^{-3} (experimental) and 104 kg m^{-3} (numerical).

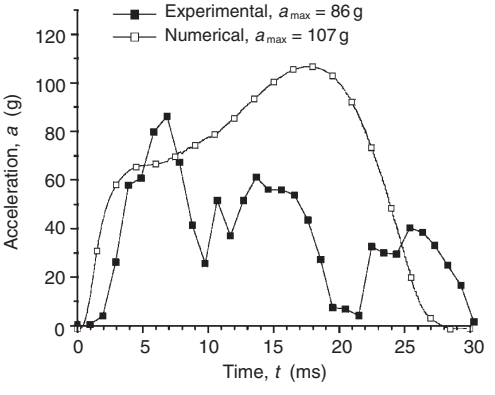

Figure 19. Comparison between experimental and numerical data for the foam of optimal density: 117 kg m^{-3} (experimental) and 104 kg m^{-3} (numerical).

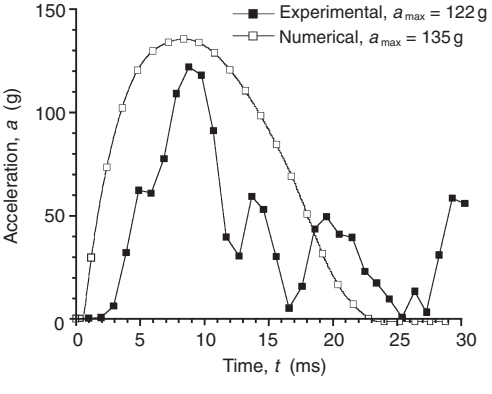

Figure 20. Comparison between experimental and numerical data for the foam of density above the value calculated as optimal by the Janssen factor method: 225 kg m^{-3} (experimental) and 200 kg m^{-3} (numerical).

be reliable and easily applicable. A material hitherto unknown from the point of view of its structural and mechanical properties could be adequately characterised using this methodology and efficiently used in the protection of packages against impacts.

REFERENCES

1. Aquaro, D. and Forasassi, G. *Analysis of the behaviour under impact loads of a shell-type shock absorber for LWR spent fuel transport packaging*. Proceedings of the International Symposium on Packaging and Transportation of Radioactive Materials, New Orleans, 1983, 1584–1590 (1983).
2. Michels, L. and Bracey, W. *The TN-MTR packaging*. Proceedings of the International Symposium on Packaging and Transportation of Radioactive Materials, Paris, 1998, 397–402 (1998).
3. Simchuk, J. D. *The design and use of the Model N-55: an individual 55 gallon drum type B overpack*. Proceedings of the International Symposium on Packaging and Transportation of Radioactive Materials, Albuquerque, 1978, 315–323 (1978).
4. Canadian Nuclear Safety Commission. *Radioactive material type B(U) package design approval certificate no. CDN/1002/B(U)*. Rev. 18 (Canada) (2001).
5. Ministry of Economy, Trade and Industry, Japan. *Certificate of approval of package design for the transport of radioactive materials*. Identification mark J/79/AF-85. Rev. 1 (Tokyo) (2001).
6. Patel, M. R. and Finnie, I. *Structural features and mechanical properties of rigid cellular plastics*. J. Cell. Plastics **5**(4), 909–932 (1970).
7. Gibson, L. and Ashby, M. F. *Cellular solids: structure and properties* (Oxford: Pergamon) ISBN 0–08–035910–8 (1988).
8. Chen, C. P. and Lakes, R. S. *Analysis of the structure–property relations of foam materials*. Cell. Polym. **14**(3), 186–202 (1995).
9. American Society for Testing and Materials. *ASTM D-1621–73: Compressive strength of rigid cellular plastics*. Annual book of ASTM standards (Philadelphia) v. 08.01 (1993).
10. Goods, S. H., Neuschwanger, C. L., Henderson, C. and Skala, D. M. *Mechanical properties and energy absorption characteristics of a polyurethane foam* (Albuquerque: Sandia National Laboratories) SAND-87–8490 (1997).
11. American Society for Testing and Materials. *ASTM D-1596–78a*: *Shock-absorbing characteristics of package-cushioning materials*. Annual book of ASTM standards (Philadelphia) v. 15.09 (1990).
12. IAEA. *Regulations for the safe transport of radioactive materials* (Vienna: IAEA) Safety Standards Series, TS-R-1 (ST-1, Rev.) (2000).
13. Woolam, W. E. *A study of the dynamics of low energy cushioning materials using scale models*. J. Cell. Plastics **4**, 79–83 (1968).
14. Ansys, Inc. *Ansys user's manual.* Version 5.3 (Houston) (1996).
15. Livermore Software Technology Corporation. *LS-DYNA version 950: User's manual* (Livermore) (1999).